Salt, Hot Water, and Silicon Compounds Tracing Massive Twin Disks

The Astrophysical Journal Letters, 900:L2 (11pp), 2020 September 1 https://doi.org/10.3847/2041-8213/abadfc

Salt, Hot Water, and Silicon Compounds Tracing Massive Twin Disks

Kei E. I. Tanaka[1,2], Yichen Zhang[3], Tomoya Hirota[1,4], Nami Sakai[3], Kazuhito Motogi[5], Kengo Tomida[2,6], Jonathan C. Tan[7,8], Viviana Rosero[9], Aya E. Higuchi[1], Satoshi Ohashi[3], Mengyao Liu[8], and Koichiro Sugiyama[1,10]
[1] National Astronomical Observatory of Japan, Mitaka, Tokyo 181-8588, Japan; kei.tanaka@nao.ac.jp
[2] Department of Earth and Space Science, Osaka University, Toyonaka, Osaka 560-0043, Japan
[3] Star and Planet Formation Laboratory, RIKEN Cluster for Pioneering Research, Wako, Saitama 351-0198, Japan
[4] Department of Astronomical Sciences, SOKENDAI (The Graduate University for Advanced Studies), Mitaka, Tokyo 181-8588, Japan
[5] Graduate School of Sciences and Technology for Innovation, Yamaguchi University, Yamaguchi 753-8512, Japan
[6] Astronomical Institute, Tohoku University, Sendai 980-8578, Japan
[7] Department of Space, Earth & Environment, Chalmers University of Technology, SE-412 96 Gothenburg, Sweden
[8] Department of Astronomy, University of Virginia, Charlottesville, VA 22904-4325, USA
[9] National Radio Astronomy Observatory, 1003 Lopezville Road, Socorro, NM 87801, USA
[10] National Astronomical Research Institute of Thailand, 260 Moo 4, T. Donkaew, A. Maerim, Chiang Mai 50180, Thailand
Received 2020 July 6; revised 2020 August 6; accepted 2020 August 10; published 2020 August 25

Abstract

We report results of 0.″05-resolution observations toward the O-type proto-binary system IRAS 16547–4247 with the Atacama Large Millimeter/submillimeter Array. We present dynamical and chemical structures of the circumbinary disk, circumstellar disks, outflows, and jets, illustrated by multi-wavelength continuum and various molecular lines. In particular, we detect sodium chloride, silicon compounds, and vibrationally excited water lines as probes of the individual protostellar disks at a scale of 100 au. These are complementary to typical hot-core molecules tracing the circumbinary structures on a 1000 au scale. The H_2O line tracing inner disks has an upper-state energy of $E_u/k > 3000$ K, indicating a high temperature of the disks. On the other hand, despite the detected transitions of NaCl, SiO, and SiS not necessarily having high upper-state energies, they are enhanced only in the vicinity of the protostars. We posit that these molecules are the products of dust destruction, which only happens in the inner disks. This is the second detection of alkali metal halide in protostellar systems after the case of the disk of Orion Source I, and also one of few massive protostellar disks associated with high-energy transition water and silicon compounds. These new results suggest that these "hot-disk" lines may be common in innermost disks around massive protostars, and have great potential for future research of massive star formation. We also tentatively find that the twin disks are counter-rotating, which might give a hint of the origin of the massive proto-binary system IRAS 16547–4247.

Unified Astronomy Thesaurus concepts: Radio jets (1347); Circumstellar disks (235); Massive stars (732); Star formation (1569); Astrochemistry (75); Binary stars (154); Protostars (1302); Young stellar objects (1834); Stellar jets (1607)

1. Introduction

Massive stars are important sources of ultraviolet (UV) radiation, turbulent energy, and heavy elements in galaxies. Massive close binaries are the progenitors of merging black holes, which are detected by their gravitational wave emission. It is of prime importance to understand the formation process of massive stars (e.g., Tan et al. 2014). An essential question is whether or not massive protostars accrete through disks, as in low-mass star formation. Recent theoretical/numerical studies support the disk accretion theory (e.g., Rosen et al. 2016; Tanaka et al. 2017; Kuiper & Hosokawa 2018). In particular, the shielding effect by the disk inside 100 au is the key to solving the longstanding radiation pressure problem (e.g., Wolfire & Cassinelli 1987) in the formation of $>40 M_\odot$ stars (Kuiper et al. 2010; Tanaka & Nakamoto 2011). Simulations also predict that an accretion disk tends to be gravitationally unstable, which results in accretion bursts (Matsushita et al. 2017; Meyer et al. 2017, 2018) and the formation of companions (Krumholz et al. 2009; Rosen et al. 2016).

Thanks to the recent development of interferometers, especially the Atacama Large Millimeter/Submillimeter Array (ALMA), more and more disk/envelope structures around massive protostars with Keplerian-like rotation have been reported (see Hirota 2018; Beltrán 2020, for recent reviews). However, so far, the number of studies reaching the resolution of $\lesssim$100 au remains limited (Hirota et al. 2017; Ginsburg et al. 2018; Maud et al. 2019; Motogi et al. 2019; Johnston et al. 2020). The hot and dense nature of the surrounding material of massive protostars leads to the detection of rich molecular lines within $<$0.1 pc, known as hot cores. One difficulty in disk hunting is the lack of knowledge of which lines can trace the innermost region and separate the disk from the envelope. Recently, there have been some attempts to identify the disk with both kinematics and chemical patterns (e.g., Zhang et al. 2019a). However, there is no agreed-upon set of such molecular lines. This work will provide a tip for the disk-tracing line selection based on new ALMA observations.

Our target IRAS 16547–4247 (hereafter IRAS 16547) is an O-type protostellar object with a bolometric luminosity of $\sim 10^5\ L_\odot$, embedded in a $10^3\ M_\odot$ clump within a radius of 0.2 pc, at the distance of 2.9 kpc (Garay et al. 2003). Radio observations showed jets aligned in a northwest–southeast direction, across a scale of 0.1 pc on the plane of the sky

(Rodríguez et al. 2005, 2008). The presence of jets indicates ongoing accretion in the vicinity of the protostar. Recently, Zapata et al. (2015, 2019) reported a binary system seen as compact dusty objects with an apparent separation of 300 au, surrounded by a circumbinary disk, using ALMA observations. Using vibrationally excited CH_3OCHO and CS transitions with upper-state energies of $E_u/k > 500$K, Zapata et al. (2019) showed that the circumbinary disk is rotating with a Keplerian-like profile of an enclosed mass of $25 \pm 3\ M_\odot$. However, the dynamics at the several $\times 100$ au scale must be controlled by the individual binary protostars, which has not been well studied.

We report new multi-band ALMA observations toward IRAS 16547 with resolutions of $0\farcs05$ at 1.3 and 3 mm. In this Letter, we mainly present the detection of sodium chloride, silicon compounds, and water lines as probes of the individual circumstellar disks. We propose that these inner-disk tracers may be common around massive protostars at the scale of $\lesssim$100 au, and valuable in understanding the disk properties in massive star formation.

2. Observations

The 3 and 1.3 mm observations were carried out with ALMA in Band 3 and 6 (ALMA project ID: 2018.1.01656.S). We also utilize the ALMA archived Band 7 (0.85 mm) data in project 2016.1.00992.S (Zapata et al. 2019). We summarize the information of the observations in Appendix Table A1. The data were calibrated using CASA (McMullin et al. 2007) pipeline v5.6.1. After pipeline calibration, we performed phase self-calibration for all the three bands using the continuum data combining line-free channels of all the spectral windows, and applied the self-calibration solutions to the line data. Images are made with CASA task tclean using the Briggs weighting with the robustness parameter of 0.5 for Band 3 and 6 data, and -0.5 for Band 7 data. The resultant synthesized beams of the continuum images are as high as $0\farcs05$ for all wavelengths (Table A1).

3. Results

3.1. Continuum

Figure 1 shows the 1.3 and 3 mm continuum maps. The dust emission dominates the 1.3 mm continuum, highlighting the circumbinary disk and outflow cavities, while the 3 mm continuum reveals the jet structures. The structures seen in the 1.3 mm continuum are very similar to those in 0.85 mm continuum (Appendix Figure B1), which was first reported by Zapata et al. (2019). Three protostars are prominent at all wavelengths, namely IRAS 16547-Ea and IRAS 16547-Eb (hereafter, sources A and B) forming the proto-binary with an apparent separation of 300 au, and a much weaker third source IRAS 16547-W. Using the 0.85 mm fluxes, which are less affected by the free–free emission than the 1.3 and 3 mm fluxes, we evaluate circumstellar disk masses of 0.19 $M_\odot$ and 0.035 $M_\odot$ around sources A and B within a radius of $0\farcs05$ (150 au) assuming a dust temperature of 350 K (Appendix B).

The proto-binary is surrounded by a circumbinary disk of 2500 au, outflow cavities are seen on the northern and southern sides of the circumbinary disk (see also Zapata et al. 2019).

The 3 mm continuum newly reveals jet knots from source A aligned in a northwest–southeast direction, which is consistent with the orientation of the central radio source detected by centimeter observations (P.A. $= -16°$; Rodríguez et al. 2005, 2008). The resolution of the ALMA observation is an order of magnitude higher than those in the previous radio observations, which allows us to spatially resolve this central radio source into sources A and B and several jet knots, and to determine that the jet originates from source A. The jet orientation is also close to the elongated distribution of water masers (Franco-Hernández et al. 2009). The prominence of the proto-binary and jet knots in 3 mm continuum suggests that they are dominated by free–free emissions, and the jet knots may also contain significant synchrotron contributions. We leave the detailed analysis of the multi-band continuum to a forthcoming paper.

3.2. Lines

Rich molecular lines are detected in IRAS 16547, especially in Bands 6 and 7. Figure 2 shows the integrated intensity maps of representative emission lines, which trace different components in the proto-binary system from the circumbinary disk to the individual circumstellar disks (see Appendix A for the summary of the lines presented in this work). Methyl cyanide CH_3CN, which is commonly used as a disk tracer toward massive protostars (e.g., Johnston et al. 2015, 2020; Beuther et al. 2017), associates with the circumbinary disk and the outflow cavity at the 1000 au scale (panels a and b). We detect the CH_3CN (12_K–11_K) K-ladder from $K = 0$ to $K = 11$ with excitation temperatures from $\sim$60 to $\sim$600 K. Here as representatives, $K = 4$ and $K = 8$ lines are shown as they are less contaminated from neighboring lines. The emission of sulfur dioxide SO_2, another typical hot-core molecule, with $E_u/k = 403$ K, also traces the circumbinary disk and the outflow cavity (panel c). However, peaks of these lower-energy transitions of CH_3CN and SO_2 with $E_u/k \lesssim 1000$ K do not coincide with the positions of sources A and B, due to self-absorption and/or absorption against the compact continuum sources in slightly redshifted velocities, indicating that they trace the outer cooler infalling material. This wide distribution makes it difficult to study the innermost regions of a few hundred au by these lines.

On the other hand, the vibrationally excited transitions of SO_2, CS, and H_2O with upper-state energies of $E_u/k \gtrsim 1000$ K trace the innermost region of the circumbinary disk and the individual protostellar disks (panels d–f). In particular, the H_2O $v_2 = 1$ emission with $E_u/k = 3464$ K is concentrated at the positions of sources A and B (panel f; the extended emission comes from contamination of other lines; see Figure 3(d)). Such a high upper-state energy reflects the high temperature of protostellar disks in massive star formation at several hundred au. With lower E_u, the SO_2 $v_2 = 1$ and CS $v = 1$ lines also trace the rotation of the circumbinary disk on the 1000 au scale (see below). We note that Zapata et al. (2019) first reported the CS $v = 1$ emission tracing the rotating circumbinary disk, but its connection to the individual circumstellar disks were not known.

Furthermore, we found that the emissions of NaCl, SiO, and SiS are also concentrated in the vicinity of the protostars (panels g–i; again the extended emissions come from contamination of other lines). These lines are not detected in the 1000 au scale, although they have the low upper-state energies of $E_u/k < 100$ K, and their critical densities of $\sim 10^6$–10^7 cm^{-3} are not high. This fact indicates that these refractory molecules are enhanced only in the innermost

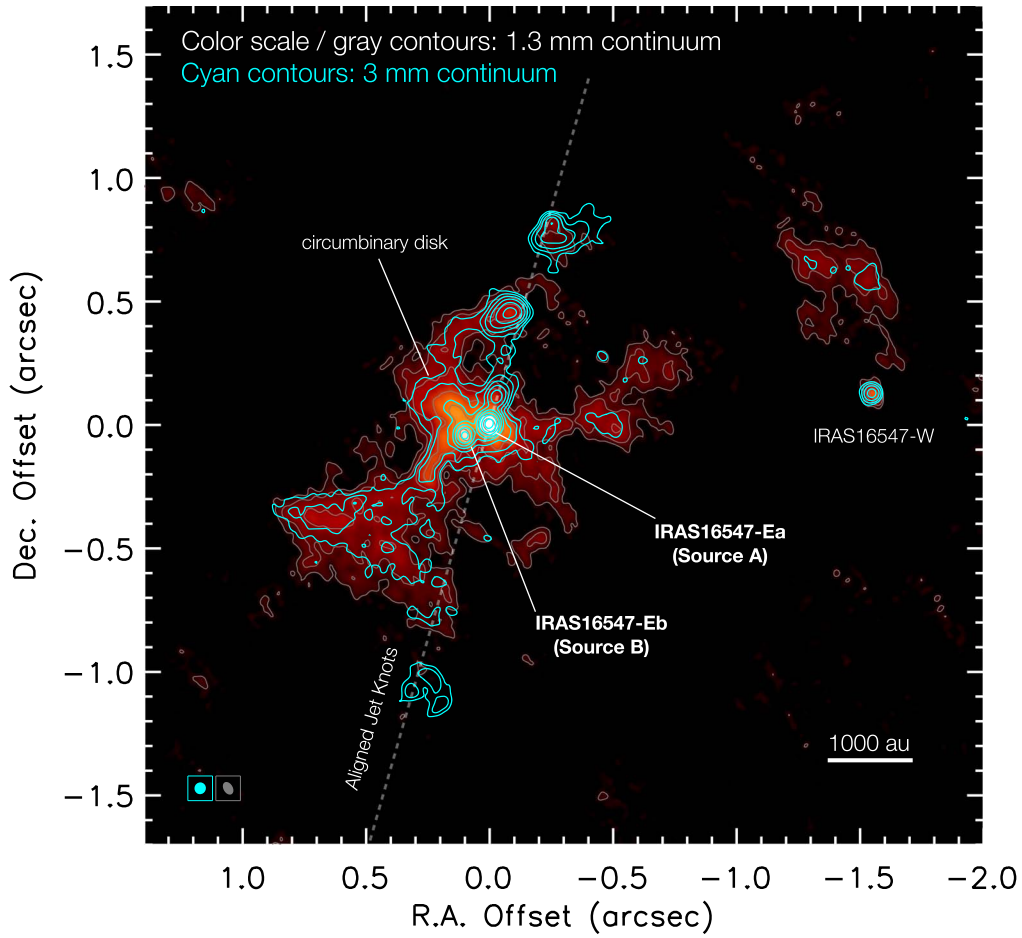

Figure 1. ALMA continuum images of IRAS 16547 at 1.3 mm (color scale and gray contours) and 3 mm (cyan contours). The contour levels are $5\sigma \times 2^n$ ($n = 0, 1,\ldots$), with $1\sigma = 0.52$ K (0.045 mJy beam^{-1}) for the 1.3 mm continuum, and $1\sigma = 0.54$ K (0.0083 mJy beam^{-1}) for the 3 mm continuum. The synthesized beams are $0\farcs055 \times 0\farcs038$ (P.A. $= 30\fdg8$) in the 1.3 mm image and $0\farcs048 \times 0\farcs046$ (P.A. $= -16\fdg8$) in the 3 mm image, respectively (shown at the lower-left corner). The R.A. and decl. offset is relative to the continuum peak position of source A, i.e., (α, δ) = ($16^{\rm h}$, $58^{\rm m}$, $17\fs2082$, $-42\arcdeg52\arcmin07\farcs421$) (ICRS). The continuum peak of source B is at ($16^{\rm h}$, $58^{\rm m}$, $17\fs2173$, $-42\arcdeg52\arcmin07\farcs461$) (ICRS).

regions of several hundred au. It is worth noting that this is the second reported detection of the alkali metal halide, NaCl, in protostellar systems after the Orion Source I disk (Ginsburg et al. 2019; Wright et al. 2020).

Appendix Table C1 summarizes the emission lines presented in this Letter. We note that some other transitions of NaCl, SiO, SiS, and vibrationally excited H_2O are also detected, which will be reported in a future paper.

Using these lines, we can illustrate the kinematics from the circumbinary disk to the individual circumstellar disks. Figure 3(a) presents the moment 1 map of the SO_2 $v_2 = 1$ line, showing the rotation of the circumbinary disk as reported by Zapata et al. (2015, 2019). The systemic velocity of IRAS 16547 is about -31 km s^{-1} (Garay et al. 2003). The rotation direction is consistent with the elongation of the circumbinary structure. Following Zapata et al. (2015, 2019), we plot the position–velocity (PV) diagrams along the major axis of the circumbinary disk (P.A. $= 50\arcdeg$), passing between sources A and B (panel b). The PV diagram of the SO_2 $v_2 = 1$ line shows a rotational profile with velocity increasing toward the center. However, inside $0\farcs1$, or 300 au, the SO_2 $v_2 = 1$ emission does not show the high-velocity component, which is expected for the Keplerian disk. Instead, the SiO emission nicely traces the central high-velocity components up to $\Delta v_{\rm lsr} \simeq \pm 30$ km s^{-1}.

Figure 3(c) shows the PV diagrams of the SO_2 $v_2 = 1$ and SiO emissions along a slit passing through sources A and B (P.A. $= -65\arcdeg$). This PV diagram is clearly not a simple Keplerian profile inside $0\farcs1$, suggesting that the two protostars dominate the dynamics at this scale. Not only the SiO line but also the SO_2 $v_2 = 1$ line shows the high-velocity components (especially in redshifted velocities) associated with sources A and B. The same is also seen in the PV diagrams of the H_2O $v_2 = 1$ emission with P.A. $= -65\arcdeg$ (panel d), where the hot-water emission prominently shows two circumstellar components. These indicate that the rotation around the binary system is smoothly connected to the rotation around the individual protostars. The two circumstellar components are not quite parallel in the PV diagrams, judging from the different direction of velocity gradient. This suggests misalignment of the rotation directions between the twin disks (see below). We note that the contaminations by other lines are seen, extending to the southeast direction at $v_{\rm lsr} \simeq -20$ and -27 km s^{-1}. We have not been able to identify these contamination lines. This source is rich in complex organic molecules, and a simultaneous check through the whole spectrum ranges is required for accurate line identification, which is left for future work.

We note that the blueshifted emission of SiO in source A is missing, probably due to self-absorption (see Figure C1 in

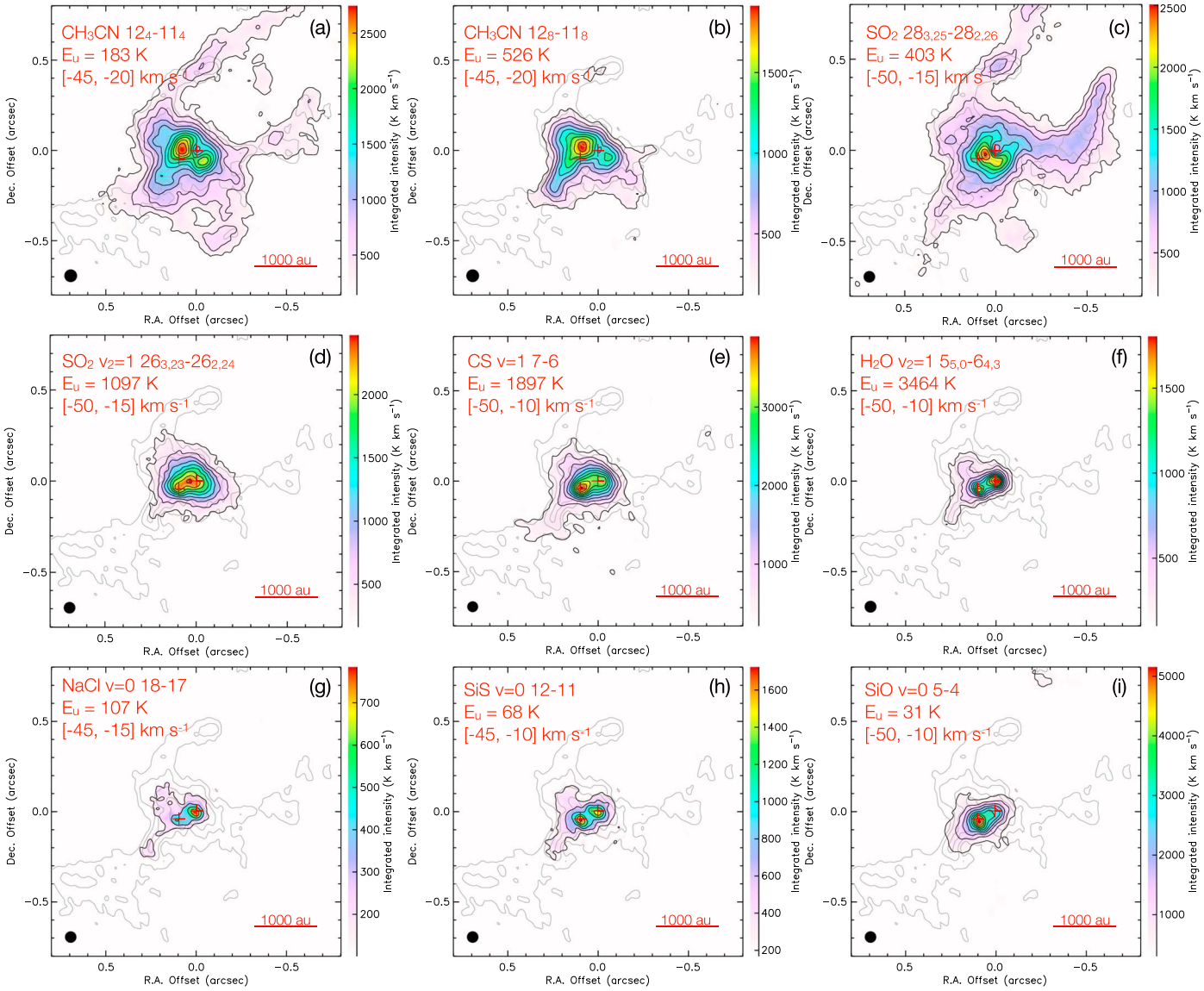

Figure 2. Integrated intensity maps of emission lines (color scale and black contours) overlaid with the 1.3 mm continuum emission (gray contours). The molecule names, transitions, upper-state energies E_u, and the integrated $v_{\rm lsr}$ ranges are labeled in each panel. The red crosses indicates the continuum peaks of sources A and B.

Appendix C), indicating that the SiO emission traces the outflowing material. However, as opposed to the commonly seen extended SiO emissions tracing shocked regions along the outflow, here the compact morphology of SiO and its close association with the two protostars suggest that it traces the material just launched from the disks or the surface layers of the disks, which can show both rotation and outflowing motions (e.g., Hirota et al. 2017; Maud et al. 2019; Zhang et al. 2019a).

Figure 4 shows the blueshifted and redshifted emissions of selected lines of water (panel a), silicon-compound (panels b–f), and sodium chloride (panels g–h). To better resolve the kinematics of the individual circumstellar disks, for the lines in Band 6, we further improve the resolution to $\sim$0.″035 ($\sim$100 au), by emphasizing data with longer baselines using a robust parameter of -0.5. For source A, the H_2O and NaCl emissions show velocity gradients in a northeast–southwest direction, which is similar to the rotation direction of the circumbinary disk (P.A. $= 50°$). Therefore, we interpret this velocity gradient as the disk rotation of source A. This orientation is also consistent with the rotating structure traced by water maser (Franco-Hernández et al. 2009) around source A. We note that this disk feature is not affected by the extended contaminations seen at $v_{\rm lsr} \simeq -20$ and -27 km s^{-1} in Figure 3(d), because they are significantly weakened by emphasizing the longer baselines. The disk A rotation is more difficult to identify in silicon-compounds emissions because these emissions could be blended with the outflowing motion. The velocity gradients of the $v = 0$ emissions of SiO and ^{30}SiO are ambiguous due to the strong absorption in the blueshifted component. For the SiO emission, comparing the redshifted emission position and the continuum peak position gives a velocity gradient direction in P.A. $\sim 10°$, which could be the outflow direction (or the direction between the outflow and the disk rotation). If this is the case, resembling the typical star formation picture, the outflow direction would be nearly perpendicular to the disk rotation, and close to parallel with the jet-knot orientation. On the other hand, the velocity gradient of the vibrationally excited ^{29}SiO line is consistent with the disk A rotation, as this line is optically thinner than the SiO $v = 0$ line

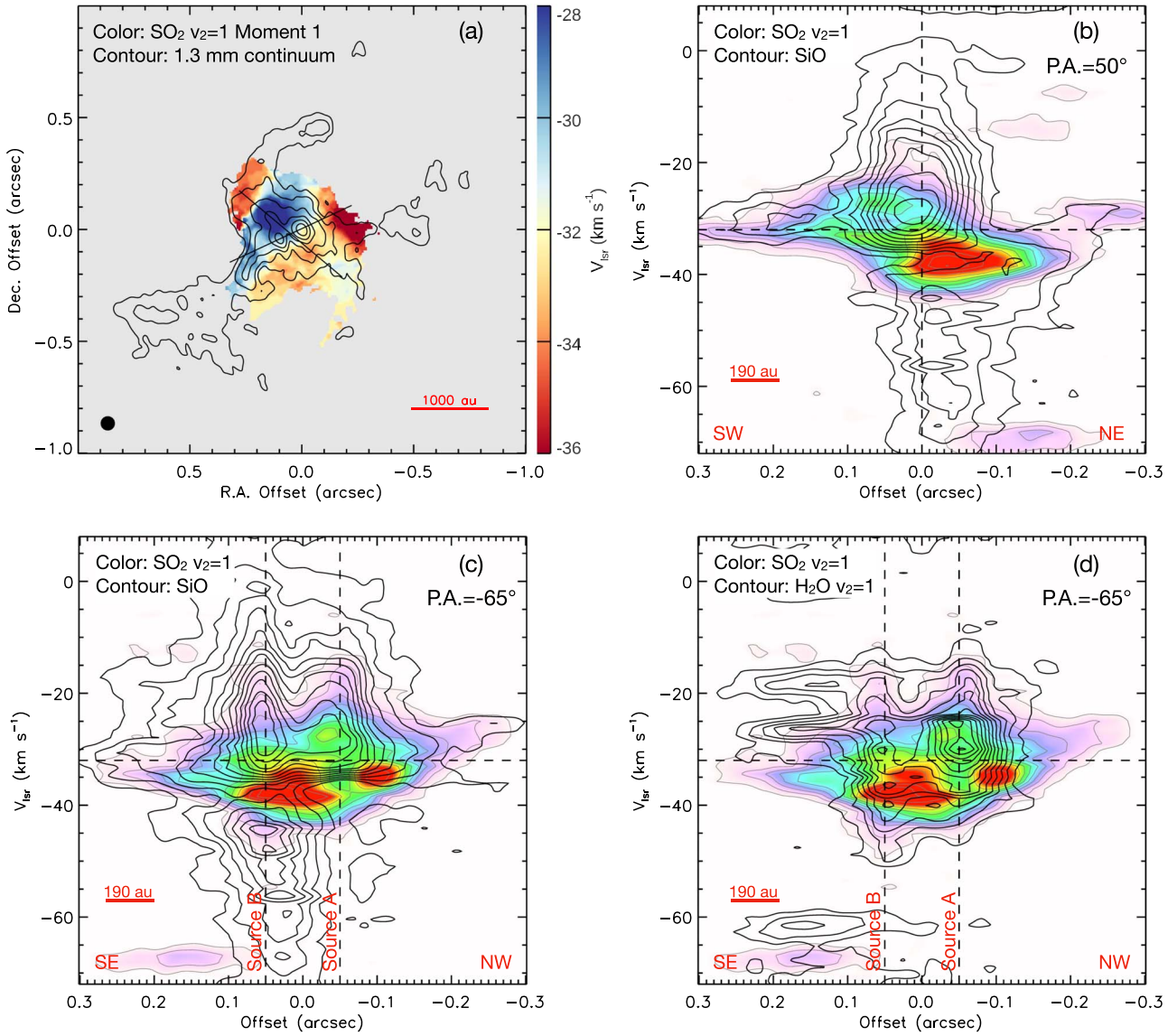

Figure 3. (a): Moment 1 map of the SO_2 $26_{3,23} - 26_{2,24}$ $v_2 = 1$ line (color scale), overlaid with the 1.3 mm continuum maps in contours (same as Figure 1(a)). The two lines show the directions along which the position–velocity (PV) diagrams shown in panels (b)–(d) are made. (b): The PV diagrams of the SO_2 $v_2 = 1$ line (color scale and thin contours) and SiO 5–4 line (thick contours), along a slit passing through the midpoint between of the two sources with P.A.=50°. The red bar in the lower-left corner indicates the resolution beam size. (c): Same as panel (b), but along a slit with P.A. = −65°. The locations of the two sources are labeled. (d): Same as panel (c), but showing the H_2O $v_2 = 1$ line in thick contours. Note that the PV diagram of H_2O is contaminated by other lines around $v_{lsr} = -20$ and -27 km s^{-1}. In panels (b)–(d), the SO_2 contours have the first level and intervals of 2.1 mJy beam^{-1}, the SiO contours have the first level and intervals of 2.2 mJy beam^{-1}, and the H_2O contours have the first level and intervals of 1.4 mJy beam^{-1}.

due to its rarity and high-excitation state. For SiS, redshifted components of $v = 0$ and 1 lines roughly follow the same velocity gradients seen by H_2O and NaCl, suggesting the existence of SiS in the disk. However, the blueshifted component is missing in the low excitation ($v = 0$) map, probably due to the similar reason for SiO. The NaCl lines trace the disk components even for the lower excitations, suggesting NaCl does not exist in the outflow unlike silicon compounds.

In source B, the velocity gradients seen in the emissions of H_2O, ^{30}SiO, ^{29}SiO, and SiS $v = 0$ are close to parallel to the disk A rotation, but in the *opposite* direction, suggesting that the circumstellar disk of source B is rotating in the opposite direction to the disk A and the circumbinary disk. The high-velocity component of the SiO $v = 0$ emission again shows a gradient perpendicular to the disk rotation, which may also trace the outflowing motion, similar to source A.

4. Discussions

4.1. Salt, Silicon Compounds, and Hot Water as Disk Probes

Based on the new high-resolution ALMA observations, we identify two groups of molecular lines tracing the innermost 100 au scale of the massive binary system IRAS 16547. The first group is the vibrationally excited "hot" lines with $E_u/k > 1000$ K. Especially, the H_2O line with $E_u/k > 3000$ K nicely traces the individual circumstellar disks. The second group is the refractory molecules, i.e., alkali halides (NaCl) and silicon compounds (SiO and SiS) in the case of IRAS 16547. The lines of refractory species do not necessarily have high excitation of >1000 K, but they trace only the innermost regions around the circumstellar disks. This fact indicates they are released to the gas phase within the disks

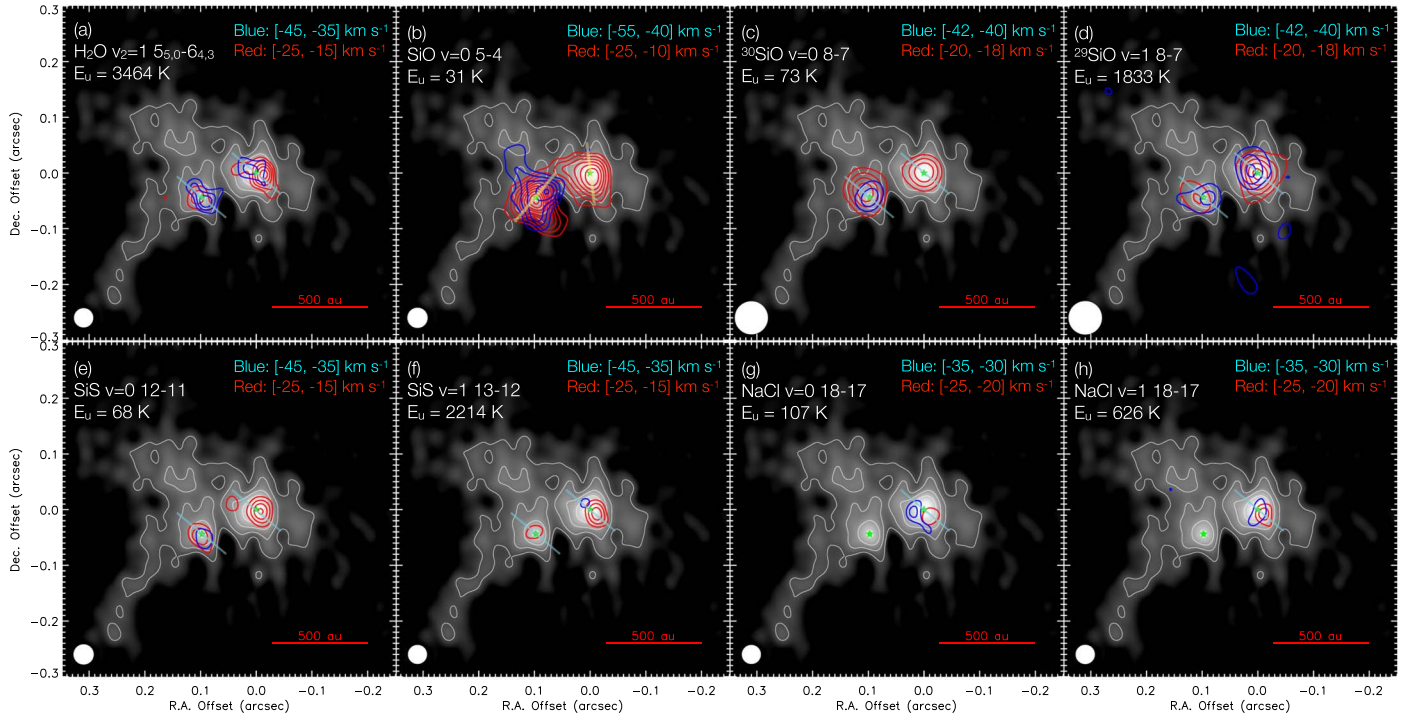

Figure 4. Integrated blueshifted and redshifted emission maps of selected inner-disk tracing molecular lines (blue and red contours) overlaid on the 1.3 mm continuum emission (grayscale and white contours). The molecule names, transitions, upper-state energies E_u, and the integrated $v_{\rm lsr}$ ranges are labeled in each panel. The stars mark the continuum peaks of sources A and B. In panels (a), (b), and (d–h), the blue and red contours have lowest contour levels of 5σ. In panel (c), the blue and red contours have lowest contour levels of 15σ and 10σ, respectively. The blue and red contour intervals are 2.5σ in all panels. Here $1\sigma =$ 92, 75, 13, 12, 61, 124, 112, 149 K km s^{-1} in panels (a–h), respectively. The cyan lines are to guide the eye of the tentative orientations of the disk rotation (panels a, and c–e), and the yellow lines for the outflows (panel b).

on the 100 au scale. The production pathway of these gas-phase refractory molecules is probably through the destruction of dust grains, e.g., sputtering under strong shocks or radiation, and thermal desorption from grain surfaces. SiO and SiS are likely released to the gas phase in the disk and then launched to the outflow, as they are associated with both the disks and the outflows. Further multi-line high-resolution observations and their excitation analysis will be crucial to investigate chemical origin of those species.

Some previous observations have reported similar molecular lines tracing the innermost regions of massive protostellar sources. Orion Source I has been intensively studied as it is the closest massive protostar candidate at a distance of 415 pc. All the disk-tracing molecules reported here, i.e., H_2O, SiO, SiS, and NaCl, are detected in Orion Source I's disk and wind launched from the disk (Hirota et al. 2012, 2014, 2017; Ginsburg et al. 2019; Wright et al. 2020). Moreover, emission lines of aluminum monoxide (AlO), one of the most refractory materials, are also found to be associated with the central region of Orion Source I (Tachibana et al. 2019). However, Orion Source I might not be the prototypical massive protostar because it has some peculiar features, e.g., the lack of an envelope, and the association of extremely strong SiO masers. Some claimed that Orion Source I could be an evolved star rather than a protostar (see Báez-Rubio et al. 2018). In either case, the single example could not establish these molecules as common disk probes of massive star formation.

Recently, in the B-type protostar G339.88–1.26, Zhang et al. (2019a) found that the disk and envelope can be disentangled not only by kinematics but also by chemical signatures. In particular, they found that the Keplerian disk is traced by SiO emission. Maud et al. (2018, 2019) also presented the SiO and vibrationally excited H_2O emissions tracing a Keplerian disk around the O-type protostar G17.64 + 0.16 at $\lesssim$100 au. Moreover, the lines of sodium chloride are detected in the disk of G17.64 + 0.16 (L. Maud 2020, private communication). In addition, in both G339.88–1.26 and G17.64 + 0.16, these authors noted that the complex organic molecules and typical hot-core lines (such as CH_3CN) trace the envelopes rather than the disks, similar to our case of IRAS 16547. Consistent with these previous findings, in the case of IRAS 16547, the individual circumstellar disks on 100 au scale are traced by the NaCl, SiS, and vibrationally excited H_2O lines. These studies suggest that hot water, silicon compounds, and alkali halides could be commonly present in dynamical and hot massive protostellar sources, and can be used to trace the inner disk and/or the material just launched from the disk. Further systematic observations are needed to confirm the common presence of those molecular lines in massive protostellar sources. Developing from the conventional hot-core chemistry, the "hot-disk" chemistry would be an essential avenue for future research of massive star formation. This work has demonstrated the usefulness of the hot-disk lines for understanding the dynamics down to $\sim$100 au from the massive protostars. We also note that the lower-energy transitions of refractory molecules are excellent targets for future radio observations by the Square Kilometre Array and the Next Generation Very Large Array, which will be able to resolve the sublimation fronts of solid materials at a 10 au scale.

An additional importance of the hot-disk chemistry around protostars is its unique link to meteoritics. The oldest materials contained in primitive meteorites, i.e., Ca-Al-rich inclusions

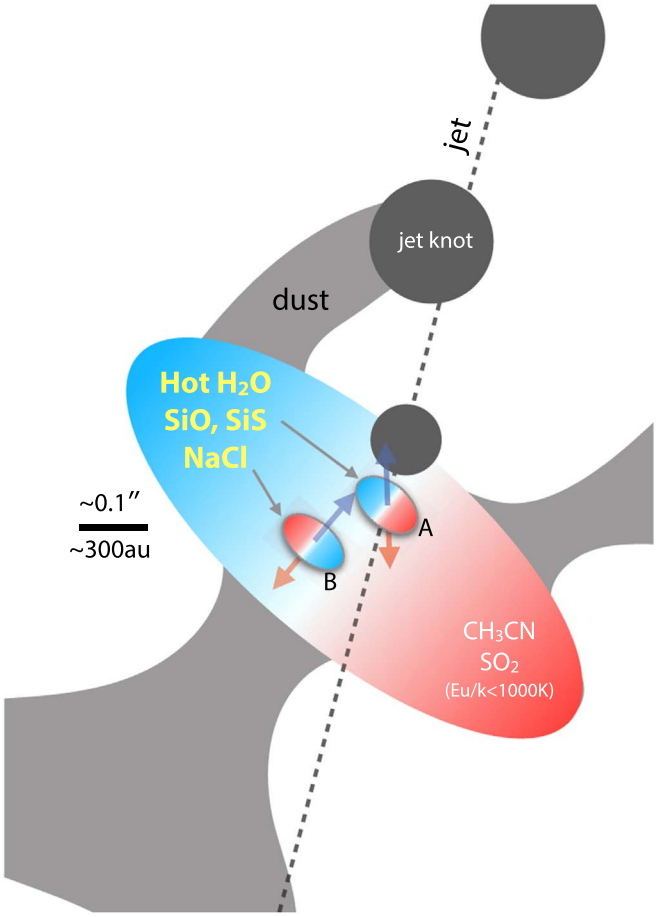

Figure 5. Schematic view of the massive proto-binary in IRAS 16547–4247. The central twin disks are revealed by high-energy transition H_2O lines with $E_u/k > 3000$ K, as well as NaCl and silicon-compound lines that are produced by the destruction of dust grains. The circumbinary disk, the dusty outflow cavity, and the jet knots are also seen by the new ALMA observations. The blue and red colors indicate the blueshifted and redshifted emissions from rotation. The circumstellar disk B is found to be counter-rotating against the disk A and the circumbinary disk. The outflowing materials from sources A and B are also traced by the SiO emission (blue and red arrows).

(CAIs) and chondrules, have been sublimated or molten once in the proto-solar disk. This fact suggests that at least some materials in the pre-solar nebula must be heated to $\gtrsim$1500 K, although protoplanetary disks are typically as cool as few hundred Kelvin in planet-forming regions of several au scale (e.g., Bell et al. 2000). Therefore, how and where CAIs and chondrules formed is still a matter of debate. Further observations of hot-disk chemistry could provide important constraints on the gas-phase conditions of refractory species, and might give unique insights into the formation of high-temperature meteoritic components.

4.2. The Massive Proto-binary IRAS 16547

Finally, we discuss the unveiled picture of the massive proto-binary IRAS 16547, and a possible scenario of its origin (see the schematics in Figure 5). The orbital dynamics could be constrained based on the systemic-velocity difference between two sources (Zhang et al. 2019b). We find the velocity difference is as small as $\Delta v_{\rm lsr} \lesssim 2$ km s^{-1} based on the available inner-disk tracing lines (Figure C1 in Appendix C). If the two protostars are coplanar with the circumbinary disk, and orbiting the same circular path following the Keplerian profile of the circumbinary disk (the enclosed mass of 25 $M_\odot$; the inclination of 55° by Zapata et al. 2019), the expected velocity difference is about 4 km s^{-1}. The fact that the observed $\Delta v_{\rm lsr}$ is smaller than the simple Keplerian velocity suggests that the protostars are gravitationally bound.

The ionized state of surrounding environments provide hints of the evolutionary stage of massive protostars (Tanaka et al. 2016; Rosero et al. 2019; Zhang et al. 2019c). Based on the free–free fluxes at 3 mm, we estimate ionizing photon rates of 9.6×10^{45} s^{-1} and 4.3×10^{45} s^{-1} for sources A and B, respectively (Appendix B). Note that those are upper limits as we ignore the contribution from dust emission. The estimated ionizing-photon rates are several orders of magnitude lower than that of zero-age main-sequence (ZAMS) stars with $>2 \times 10^4$ $L_\odot$ (Davies et al. 2011), suggesting that the binary stars are at protostar phase with large radii of $\sim$20 $R_\odot$. The evolutionary calculations of protostars proposed that such large radii of massive protostars are the consequence of high accretion rates of $\gtrsim 10^{-4} M_\odot$ yr^{-1} (e.g., Hosokawa & Omukai 2009; Haemmerlé et al. 2016).

Although the free–free emission has been detected in IRAS 16547 at radio wavelengths (Rodríguez et al. 2005, 2008), we do not detect hydrogen recombination lines such as H40α and H42α. The non-detection of recombination lines can be explained by the line broadening with a width of $\gtrsim$100 km s^{-1} (Appendix B), which is consistent with the presence of jets seen in the 3 mm continuum. Additionally, the northern jet knots are located with approximately equal intervals of 0.″4, or 1000 au, which may be evidence of periodic accretion induced by a hidden companion or some disk instability around source A. Assuming a total mass of 20 $M_\odot$ and a jet velocity of 100 km s^{-1} on the sky plane, we estimate this hidden companion should have a period of 50 yr and a semimajor axis of 40 au. The proper motion of the jet knots would be detectable by follow-up observations with similar resolutions, which will provide important clues for testing the companion's presence and for understanding jet launching and precession (Rodríguez et al. 2008).

The two protostars have similar continuum fluxes and line emissions, and look coplanar with the circumbinary disk. Those features superficially link to the disk fragmentation as the origin of the binary system (e.g., Krumholz et al. 2009). A puzzling finding, however, is the tentative detection of the counter-rotating disks (Figure 4), which are difficult to form by disk fragmentation. An alternative mechanism is turbulent fragmentation at the molecular cloud-core scale (e.g., Offner et al. 2010; Bate 2012; Kuffmeier et al. 2019). Although their birthplaces may be distant, some pairs of protostars can migrate to as close as $\lesssim$100 au, forming binary systems. The presence of turbulence leads to the random rotation of protostellar disks, which remains even after the migration (Offner et al. 2016). The turbulent fragmentation scenario would go well with the small-cluster nature of IRAS 16547 on the scale of $\lesssim$0.1 pc, seen in the misalignments of several outflows and jets (Higuchi et al. 2015). However, considering the actual origin of binary systems could be much more complicated, e.g., the combination of both fragmentation processes (Rosen & Krumholz 2020) and the dynamical interactions with highly eccentric orbits (Saiki & Machida 2020), it is difficult to conclude the formation process based on the currently available information. We want to emphasize that the detection of the counter-rotation

is still tentative, and follow-up high-resolution observations are required to conclude the disk orientations of IRAS 16547.

5. Summary

We report the dynamical and chemical structures of the massive proto-binary system IRAS 16547–4247 using 0.″05-resolution ALMA observations at 3, 1.3, and 0.85 mm. We propose that (1) the lines of destructed-dust molecules, such as alkali metal halides (e.g., NaCl) and silicon compounds (e.g., SiO and SiS), and (2) the high-excitation water line with $E_u/k > 3000$ K, can act as good tracers for investigating dynamics of the innermost region of massive star formation at a scale of $\lesssim$100 au.

Figure 5 shows the schematic view of the proto-binary IRAS 16547 presented in this study. In the scale of 1000 au, the rotation of the circumbinary disk is revealed by emission lines of typical hot-core molecules, such as CH_3CN and SO_2, with upper-state energies of $E_u/k \simeq$ 100–1000 K (Zapata et al. 2019). However, these lines cannot trace well the protostellar disks at a 100 au scale. Instead, we found that some molecular lines, including vibrationally excited water, silicon compounds, and sodium chloride, exclusively trace the individual circumstellar disks. The detection of vibrationally excited lines in H_2O, SiO, SiS, and NaCl with upper-state energy as high as >2000–3000 K indicates a very high temperature in the innermost disks. Because sodium chloride and silicon compounds are produced through the destruction of dust grains in the dynamical disks, their emissions are seen only in the vicinity of protostars, even for the lower-energy transitions with $E_u/k < 100$ K. Using these new disk probes, we analyzed the disk kinematics and tentatively discovered that the twin disks are counter-rotating. The pair of the counter-rotating disks might suggest that the binary system is formed via turbulent fragmentation at the cloud-core scale rather than disk fragmentation. However, more observations are needed to confirm the rotation directions of disks.

Notably, this is the second reported detection of salt in protostellar systems after the case of the disk of Orion Source I (Ginsburg et al. 2019), and also one of few massive protostellar disks associated with high-energy transition water and silicon compounds (e.g., Maud et al. 2018, 2019; Zhang et al. 2019a). These new results suggest these "hot-disk" lines may be common in innermost disks around massive protostars and can be detected in high-resolution observations. Such "hot-disk" chemistry has great potential for the future research of massive star formation.

The authors thank T. Nakamoto, M. Kobayashi, L. Maud, and A. Ginsburg for fruitful discussions. The authors also thank the anonymous referee for providing insightful comments. This Letter makes use of the following ALMA data: ADS/JAO.ALMA#2016.1.00992.S., and ADS/JAO.ALMA#2018.1.01656.S. ALMA is a partnership of ESO (representing its member states), NSF (USA) and NINS (Japan), together with NRC (Canada), MOST and ASIAA (Taiwan), and KASI (Republic of Korea), in cooperation with the Republic of Chile. The Joint ALMA Observatory is operated by ESO, AUI/NRAO and NAOJ. This research is supported by NAOJ ALMA Scientific Research grant No. 2017-05A (K.E.I.T. and K.T.), RIKEN Special Postdoctoral Researcher Program (Y.Z.), ERC project MSTAR, VR grant 2017-04522 (J.C.T), JSPS KAKENHI grant Nos. JP19H05080, 19K14760 (K.E.I.T.), 19K14774 (Y.Z.), 17K05398 (T.H.), 19H05082, 19H01937 (K.M.), 16H05998, 17KK0091, 18H05440 (K.T.), and 20K14533 (S.O.).

Software: CASA (http://casa.nrao.edu, McMullin et al. 2007), the IDL Astronomy User's Library (https://idlastro.gsfc.nasa.gov; Landsman 1995).

Appendix A
Information of the Observations

Table A1 summarizes the information of the observations of Band 3, 6 (project: 2018.1.01656.S), and 7 (project

Table A1
Information of the Observations

Band	Obs. Date (Total Time)	# of Ant.	Baseline Range	Phase Cal.	Flux/Bandpass Cal.	$\theta_{\rm beam}$[a]	$\theta_{\rm MRS}$[b]
3	2019 Jun 9 (90 minutes)	45	83.1 m–16.2 km	J1706-4600	J1617-5848	0.″048 × 0.″046	0.″73
6	2019 Jul 15 (78 minutes)	42	138.5 m–8.5 km	J1706-4600	J1427-4206	0.″055 × 0.″038	0.″75
7	2019 Aug 21–22 (100 minutes)	44	21.0 m–3.7 km	J1636-4102	J1617-5848/J1427-4206	0.″056 × 0.″046	0.″84

Notes.
[a] The synthesized beams for the continuum images. A robust weighting parameter of 0.5 is used for Band 3 and 6 data, and a robust weighting parameter of −0.5 is used for Band 7 data.
[b] The maximum recoverable scales.

2016.1.00992.S, Zapata et al. 2019). As listed, similar high resolutions of ∼0.″05 are achieved for all wavelengths.

Appendix B
Estimations of Protostellar Properties

We estimate the properties of the protostars based on results of multi-wavelength ALMA observations. The disk masses can be estimated using the dust flux of $S_{\nu,d}$,

$$M_{\rm disk} = \frac{D^2\Omega}{\kappa_{\nu,d}} \log\left(1 - \frac{S_{\nu,d}}{B_\nu(T_d)\Omega}\right)^{-1}, \quad \text{(B1)}$$

where $D = 2.9$ kpc is the distance to IRAS 16547, Ω is the solid angle of the integrated region, $\kappa_{\nu,d}$ is the dust opacity per gas mass, and $B_\nu(T_d)$ is the Planck function at the dust temperature T_d, respectively. We utilize the 0.85 mm fluxes of $S_{\nu,d} = 84$ and 60 mJy within 0.″05 for sources A and B, because the dust emission should dominate at this wavelength (Figure B1). The dust temperatures in the disks are uncertain from the currently available data, but the peak brightness temperature of 340 K at 0.85 mm suggests the high temperature of $T_d \gtrsim 350$ K. Here we assume the dust temperature range of $T_d = 350$–500 K. Considering the physical condition of the disks, we apply the dust opacity of $\kappa_{\nu,d} = 0.097$ cm^2 g^{-1} for the coagulated dust model in the high density of 10^8 cm^{-3} without the ice mantle (Ossenkopf & Henning 1994; a gas-to-dust ratio of 100 is assumed). We evaluate the disks masses as 0.033–0.19 $M_\odot$ and 0.019–0.035 $M_\odot$ for sources A and B, respectively, at the dust temperature range of $T_d = 350$–500 K.

The free–free emissions at radio wavelengths are observed at the center of IRAS16547 (Rodríguez et al. 2005, 2008), suggesting the existence of photoionized regions. Under the assumption of the optically thin free–free emission, we can evaluate the ionizing-photon rates of the protostars (Schmiedeke et al. 2016),

$$S_{\rm ion} = 4.771 \times 10^{42} \left(\frac{S_{\nu,\rm ff}}{\rm Jy}\right)\left(\frac{T_e}{\rm K}\right)^{-0.45}\left(\frac{\nu}{\rm GHz}\right)^{0.1}\left(\frac{D}{\rm pc}\right)^2 {\rm s}^{-1}, \quad \text{(B2)}$$

where T_e is the electron temperature, which we use the typical values of 8000 K (Keto et al. 2008). We adopt the 3 mm continuum for the free–free fluxes, which is the upper limit because the dust emission would contribute. Based on $S_{\nu,\rm ff} = 36$ and 17 mJy within 0.″05, we evaluate the ionizing-photon rates of 9.7×10^{45} s^{-1} and 4.3×10^{45} s^{-1} for sources A and B, respectively. The evaluated rates are orders of magnitude lower than ZAMS stars with luminosities $>2 \times 10^4$ $L_\odot$ (Davies et al. 2011; note the total luminosity of IRAS 16547 is $\sim 10^5$ $L_\odot$), confirming that sources A and B are still at the protostellar phase with large radii. Assuming the

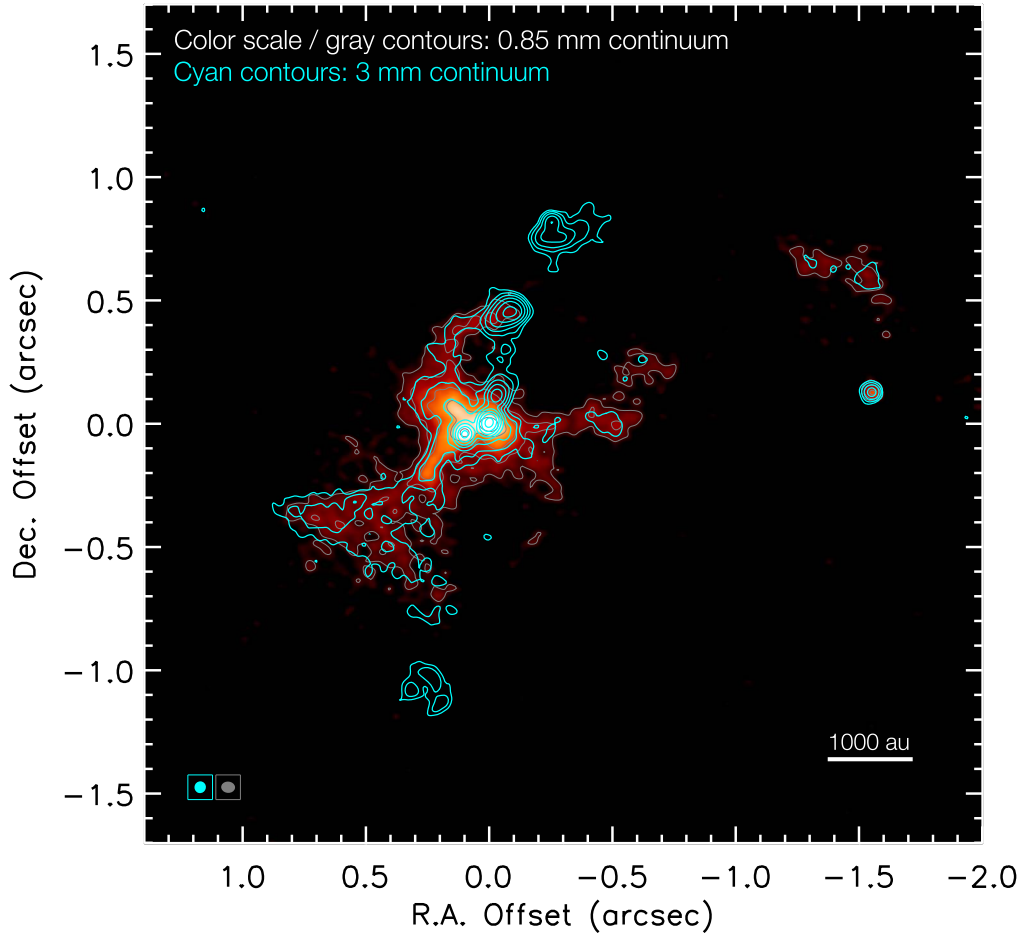

Figure B1. Same as Figure 1, but showing the 0.85 mm continuum image in color scale and gray contours. The contour levels are $5\sigma \times 2^n$ ($n = 0, 1, \ldots$), with $1\sigma = 1.6$ K (0.40 mJy beam^{-1}). The synthesized beam is 0.″056 × 0.″046 (P.A.=85.°9) for the 0.85 mm continuum image (shown at the lower-left corner).

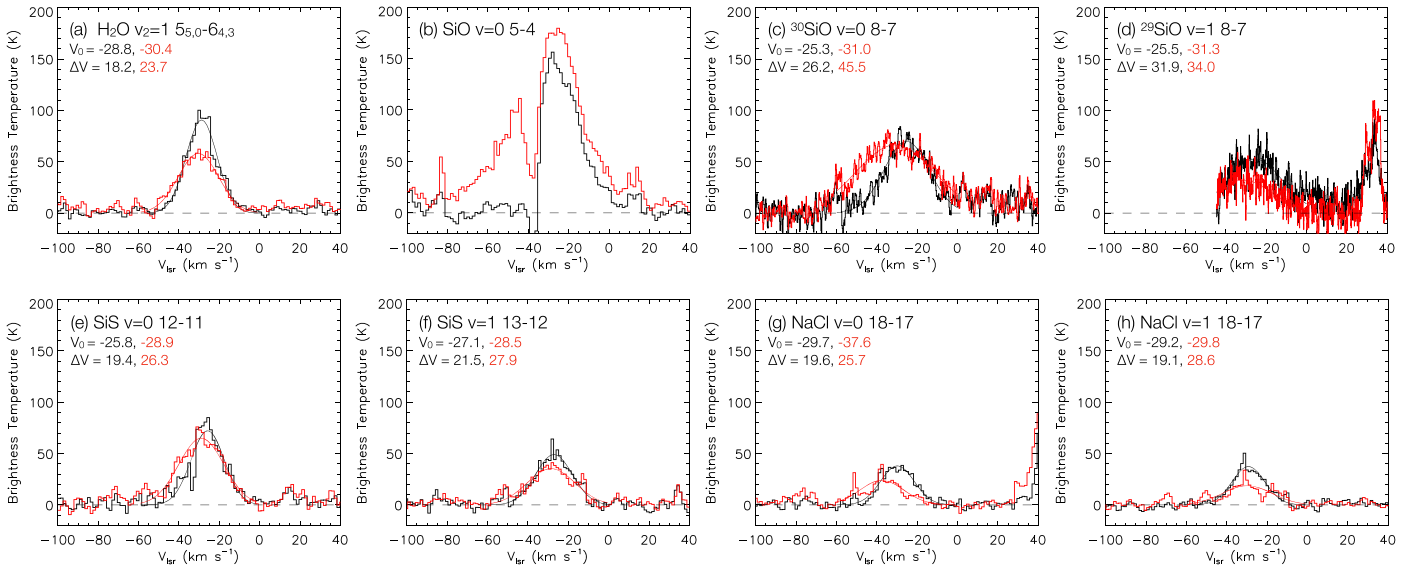

Figure C1. Line spectra of water, silicon compounds, and sodium chloride at the continuum peak positions of sources A (red) and B (black). The fitted Gaussian functions are also displayed with their central and FMHW velocities in the unit of km s^{-1}, V_0 and ΔV, except for the SiO (5–4) emission with the strong absorption.

bolometric luminosities are $5 \times 10^4\ L_\odot$, we estimate the stellar radii of 16 $R_\odot$ and 17 $R_\odot$ for sources A and B, respectively (Tanaka et al. 2016). Such large radii of the massive protostars suggest that both protostars have grown with high accretion rates $\gtrsim 10^{-4} M_\odot$ yr^{-1} (e.g., Hosokawa & Omukai 2009; Haemmerlé et al. 2016).

We do not identify the hydrogen recombination lines of H26α, H30α, H40α, and H42α (353.6227, 231.9009, 99.0230, and 85.6884 GHz, respectively), which suggests a broadening effect due to the high-velocity jets. Under the assumption of the optically thin and local thermal equilibrium conditions of the recombination lines, we can estimate the the ratio of hydrogen recombination lines to the free–free continuum (Anglada et al. 2018),

$$\frac{I_{\nu,\mathrm{HRL}}}{I_{\nu,\mathrm{ff}}} = 0.19\left(\frac{\nu}{\mathrm{GHz}}\right)^{1.1}\left(\frac{T_e}{10^4\ \mathrm{K}}\right)^{-1.1}\left(\frac{\Delta V}{\mathrm{km\ s^{-1}}}\right)^{-1}(1+Y^+)^{-1}, \quad \text{(B3)}$$

where Y^+ is the ratio of the He^+ and H^+ column densities (we use the typical value of $Y^+ = 0.08$). Again, we adopt the 3 mm continuum flux as the free–free emission. Taking into account the peak intensity $I_{\nu,\mathrm{ff}} = 7.2$ mJy beam^{-1} and the rms noise of 0.4 mJy beam^{-1}, we estimated that the line width would be $\Delta V \gtrsim 100$ km s^{-1} for the non-detection with 5σ level, i.e., $I_{\nu,\mathrm{HRL}} < 2$ mJy beam^{-1}. This wide width is consistent with the presence of the jets. We note that this is a conservative limit because the 3 mm flux also contains the dust emission.

Appendix C
Information of the Presented Molecular Lines

Table C1 summarizes the emission lines presented in this study. We particularly discuss the detection of sodium chloride, silicon compounds, and hot water as the disk probes at the 100 au scale. Figure C1 shows the spectra of these emissions at the continuum peaks of sources A and B. The fitted Gaussian functions of each profile are also presented, except for the SiO (5–4) emission, which has strong absorption. The systemic velocity of IRAS 16547 is about -31 km s^{-1} (Garay et al. 2003). As seen in Figure 4, the individual disks are traced particularly well by the emissions of H_2O, NaCl ($v = 0$, 1), and SiS ($v = 1$) for source A, and H_2O, and SiS ($v = 0$) for source B. These lines have quasi-Gaussian shapes with FMHWs of 18–26 km s^{-1}. We do not identify a clear line-of-sight velocity difference between the two protostars, i.e., $\Delta v_{\mathrm{lsr}} \lesssim 2$ km s^{-1}, which indicates that the binary system is gravitationally bound (Section 4.2). The water line is contaminated by the other lines at around $v_{\mathrm{lsr}} = -20$ and -27 km s^{-1} (see also Figure 3(d)), which we have not been able to identify. On the other hand, the SiO (5–4) emission traces not only the disks but also the outflows. Thus, it is broader with clear absorption features in the blueshifted side (see also Figure 2(h) and (i)). Similar features are also seen in some of the other silicon-compound lines, e.g., SiS ($v = 0$) and

Table C1
Molecular Lines Presented in This Letter

Molecule	Transition	Frequency (GHz)	E_u/k (K)	$S\mu^2$ (D^2)
H_2O	$5_{5,0}$–$6_{4,3}$ ($v_2 = 1$)	232.6867000	3463.6	1.079
SiO	5–4 ($v = 0$)	217.1049800	31.3	48.00
^{30}SiO	8–7 ($v = 0$)	338.9300437	73.2	76.81
^{29}SiO	8–7 ($v = 1$)	340.6118622	1832.6	77.77
SiS	12–11 ($v = 0$)	217.8176630	68.0	12.55
SiS	13–12 ($v = 1$)	234.8129678	1150.6	169.5
NaCl	18–17 ($v = 1$)	232.5099753	626.0	1478
NaCl	18–17 ($v = 0$)	234.2519153	106.9	1458
CH_3CN	12_4–11_4	220.6792874	183.2	328.2
CH_3CN	12_8–11_8	220.4758078	525.8	205.1
SO_2	$28_{3,25}$–$28_{2,26}$ ($v = 0$)	234.1870566	403.2	55.09
SO_2	$26_{3,23}$–$26_{2,24}$ ($v_2 = 1$)	216.7585584	1096.5	54.13
CS	7–6 ($v = 1$)	340.3979569	1896.6	26.24

Note. Line information of H_2O is taken from the Jet Propulsion Laboratory line database (Pickett et al. 1998), the information of other lines are taken from the Cologne Database for Molecular Spectroscopy molecular line catalog (Müller et al. 2005). The molecular lines listed above the horizontal line between NaCl and CH_3CN trace well the 100 au scales of IRAS16547 (see Figures 4 and C1).

^{30}SiO of source A. The deeper absorptions in the silicon-compound lines in source A suggests its stronger outflow than the outflow B.

ORCID iDs

Kei E. I. Tanaka https://orcid.org/0000-0002-6907-0926
Yichen Zhang https://orcid.org/0000-0001-7511-0034
Tomoya Hirota https://orcid.org/0000-0003-1659-095X
Nami Sakai https://orcid.org/0000-0002-3297-4497
Kazuhito Motogi https://orcid.org/0000-0002-3789-770X
Kengo Tomida https://orcid.org/0000-0001-8105-8113
Jonathan C. Tan https://orcid.org/0000-0002-3389-9142
Viviana Rosero https://orcid.org/0000-0001-8596-1756
Aya E. Higuchi https://orcid.org/0000-0002-9221-2910
Satoshi Ohashi https://orcid.org/0000-0002-9661-7958
Mengyao Liu https://orcid.org/0000-0001-6159-2394
Koichiro Sugiyama https://orcid.org/0000-0002-6033-5000

References

Anglada, G., Rodríguez, L. F., & Carrasco-González, C. 2018, A&ARv, 26, 3
Báez-Rubio, A., Jiménez-Serra, I., Martín-Pintado, J., et al. 2018, ApJ, 853, 4
Bate, M. R. 2012, MNRAS, 419, 3115
Bell, K. R., Cassen, P. M., Wasson, J. T., et al. 2000, in Protostars and Planets IV, ed. V. Mannings, A. P. Boss, S. S. Russell et al. (Tucson, AZ: Univ. Arizona Press), 897
Beltrán, M. 2020, The Star Formation Newsletter, 329, 1, arXiv:2005.06912
Beuther, H., Walsh, A. J., Johnston, K. G., et al. 2017, A&A, 603, A10
Davies, B., Hoare, M. G., Lumsden, S. L., et al. 2011, MNRAS, 416, 972
Franco-Hernández, R., Moran, J. M., Rodríguez, L. F., et al. 2009, ApJ, 701, 974
Garay, G., Brooks, K. J., Mardones, D., et al. 2003, ApJ, 587, 739
Ginsburg, A., Bally, J., Goddi, C., et al. 2018, ApJ, 860, 119
Ginsburg, A., McGuire, B., Plambeck, R., et al. 2019, ApJ, 872, 54
Haemmerlé, L., Eggenberger, P., Meynet, G., et al. 2016, A&A, 585, A65
Higuchi, A. E., Saigo, K., Chibueze, J. O., et al. 2015, ApJL, 798, L33
Hirota, T. 2018, PKAS, 33, 21
Hirota, T., Kim, M. K., & Honma, M. 2012, ApJL, 757, L1
Hirota, T., Kim, M. K., Kurono, Y., et al. 2014, ApJL, 782, L28
Hirota, T., Machida, M. N., Matsushita, Y., et al. 2017, NatAs, 1, 0146
Hosokawa, T., & Omukai, K. 2009, ApJ, 691, 823
Johnston, K. G., Hoare, M. G., Beuther, H., et al. 2020, A&A, 634, L11
Johnston, K. G., Robitaille, T. P., Beuther, H., et al. 2015, ApJL, 813, L19
Keto, E., Zhang, Q., & Kurtz, S. 2008, ApJ, 672, 423
Krumholz, M. R., Klein, R. I., McKee, C. F., Offner, S. S. R., & Cunningham, A. J. 2009, Sci, 323, 754
Kuffmeier, M., Calcutt, H., & Kristensen, L. E. 2019, A&A, 628, A112
Kuiper, R., & Hosokawa, T. 2018, A&A, 616, A101
Kuiper, R., Klahr, H., Beuther, H., & Henning, T. 2010, ApJ, 722, 1556
Landsman, W. B. 1995, in ASP Conf. Ser. 77, Astronomical Data Analysis Software and Systems IV, ed. R. A. Shaw, H. E. Payne, & J. J. E. Hayes (San Francisco, CA: ASP), 437
Matsushita, Y., Machida, M. N., Sakurai, Y., et al. 2017, MNRAS, 470, 1026
Maud, L. T., Cesaroni, R., Kumar, M. S. N., et al. 2018, A&A, 620, A31
Maud, L. T., Cesaroni, R., Kumar, M. S. N., et al. 2019, A&A, 627, L6
McMullin, J. P., Waters, B., Schiebel, D., Young, W., & Golap, K. 2007, in ASP Conf. Ser. 376, Astronomical Data Analysis Software and Systems XVI, ed. R. A. Shaw, F. Hill, & D. J. Bell (San Francisco, CA: ASP), 127
Meyer, D. M.-A., Kuiper, R., Kley, W., et al. 2018, MNRAS, 473, 3615
Meyer, D. M.-A., Vorobyov, E. I., Kuiper, R., et al. 2017, MNRAS, 464, L90
Motogi, K., Hirota, T., Machida, M. N., et al. 2019, ApJL, 877, L25
Müller, H. S. P., Schlöder, F., Stutzki, J., et al. 2005, JMoSt, 742, 215
Offner, S. S. R., Dunham, M. M., Lee, K. I., et al. 2016, ApJL, 827, L11
Offner, S. S. R., Kratter, K. M., Matzner, C. D., et al. 2010, ApJ, 725, 1485
Ossenkopf, V., & Henning, T. 1994, A&A, 291, 943
Pickett, H. M., Poynter, R. L., Cohen, E. A., et al. 1998, JQSRT, 60, 883
Rodríguez, L. F., Garay, G., Brooks, K. J., et al. 2005, ApJ, 626, 953
Rodríguez, L. F., Moran, J. M., Franco-Hernández, R., et al. 2008, AJ, 135, 2370
Rosen, A. L., & Krumholz, M. R. 2020, AJ, 160, 78
Rosen, A. L., Krumholz, M. R., McKee, C. F., et al. 2016, MNRAS, 463, 2553
Rosero, V., Tanaka, K. E. I., Tan, J. C., et al. 2019, ApJ, 873, 20
Saiki, Y., & Machida, M. N. 2020, ApJL, 897, L22
Schmiedeke, A., Schilke, P., Möller, T., et al. 2016, A&A, 588, A143
Tachibana, S., Kamizuka, T., Hirota, T., et al. 2019, ApJL, 875, L29
Tan, J. C., Beltrán, M. T., Caselli, P., et al. 2014 (Protostars and Planets VI) ed. H. Beuther et al. (Tucson, AZ: Univ. Arizona Press), 149
Tanaka, K. E. I., & Nakamoto, T. 2011, ApJL, 739, L50
Tanaka, K. E. I., Tan, J. C., & Zhang, Y. 2016, ApJ, 818, 52
Tanaka, K. E. I., Tan, J. C., & Zhang, Y. 2017, ApJ, 835, 32
Wolfire, M. G., & Cassinelli, J. P. 1987, ApJ, 319, 850
Wright, M., Plambeck, R., Hirota, T., et al. 2020, ApJ, 889, 155
Zapata, L. A., Garay, G., Palau, A., et al. 2019, ApJ, 872, 176
Zapata, L. A., Palau, A., Galván-Madrid, R., et al. 2015, MNRAS, 447, 1826
Zhang, Y., Tan, J. C., Sakai, N., et al. 2019a, ApJ, 873, 73
Zhang, Y., Tan, J. C., Tanaka, K. E. I., et al. 2019b, NatAs, 3, 517
Zhang, Y., Tanaka, K. E. I., Rosero, V., et al. 2019c, ApJL, 886, L4